© 2017 IJSRSET | Volume 3 | Issue 2 | Print ISSN: 2395-1990 | Online ISSN : 2394-4099
Themed Section: Engineering and Technology

Development of Special elements in hybrid FEM

Yi Xiao

Research School of Engineering, Australian National University, Acton, ACT 2601, Australia

ABSTRACT

This paper presents an overview on developments of special elements in hybrid finite element method (FEM). Recent developments on special elements of the hybrid FEM are described. Formulations for all cases are derived by means of modified variational functional and fundamental solutions or Trefftz functions. Generation of elemental stiffness equations from the modified variational principle is also discussed. Finally, a brief summary of the approach and potential research topics is provided.

Keywords: Finite Element Method, Fundamental Solution, Special Element.

I. INTRODUCTION

Cellular solids like honeycombs, foams, films, cancellous bone, etc., are of considerable interest in engineering applications due to their superior thermal and mechanical performance [1-6]. It should be mentioned that analytical solutions which are available only for a few problems with simple geometries and boundary conditions [7-21]. Therefore, development of efficient numerical methods is vital for solving engineering problems [22-28]. The first is the so-called hybrid Trefftz FEM (or H-Trefftz method) [29, 30]. Unlike in the conventional FEM, the H-Trefftz method couples the advantages of conventional FEM [31-34] and BEM [35-37]. In contrast to the standard FEM, the H-Trefftz method is based on a hybrid method which includes the use of an independent auxiliary inter-element frame field defined on each element boundary and an independent internal field chosen so as to a prior satisfy the homogeneous governing differential equations by means of a suitable truncated T-complete function set of homogeneous solutions. Since 1970s, H-Trefftz model has been considerably improved and has now become a highly efficient computational tool for the solution of complex boundary value problems. It has been applied to potential problems [38-41], two-dimensional elastics [42, 43], elastoplasticity [44, 45], fracture mechanics [46-48], micromechanics analysis [49, 50], problem with holes [51, 52], heat conduction [53-55], thin plate bending [56-59], thick or moderately thick plates [60-64], three-dimensional problems [65], piezoelectric materials [66-70], and contact problems [71-73].

On the other hand, the hybrid FEM based on the fundamental solution (F-Trefftz method for short) was initiated in 2008 [30, 74] and has now become a very popular and powerful computational methods in mechanical engineering. The F-Trefftz method is significantly different from the T-Trefftz method discussed above. In this method, a linear combination of the fundamental solution at different points is used to approximate the field variable within the element. The independent frame field defined along the element boundary and the newly developed variational functional are employed to guarantee the inter-element continuity, generate the final stiffness equation and establish linkage between the boundary frame field and internal field in the element. This review will focus on the F-Trefftz finite element method.

The F-Trefftz finite element method, newly developed recently [30, 74], has gradually become popular in the field of mechanical and physical engineering since it is initiated in 2008 [30, 75, 76]. It has been applied to potential problems [40, 77-79], plane elasticity [43, 80, 81], composites [82-87], piezoelectric materials [88-90], three-dimensional problems [91], functionally graded materials [92-94], bioheat transfer problems [95-101], thermal elastic problems [102], hole problems [103, 104], heat conduction problems [74, 105], micromechanics problems [49, 50], and anisotropic elastic problems [106-109].

Following this introduction, the present review consists of 3 sections. Special F-Trefftz elements for plane elasticity with circular holes are described in Section 2. It describes in detail the method of deriving element stiffness equations. Section 3 focuses on the essentials of special elliptical hole elements. Section 4 presented Special elements for plane elasticity with discontinuous loads. Finally, a brief summary of the developments of the hybrid methods is provided.

II. METHODS AND MATERIAL

A. Special Circular Elements

1. Basic equations for plane elasticity

For a well-posed plane elastic problem with circular cutouts in an arbitrary domain Ω, as shown in Figure 1, the corresponding partial differential governing equations under the assumption of small deformation are given in matrix form as

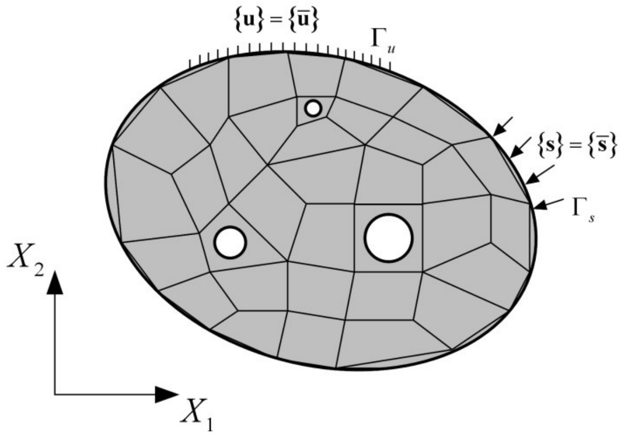

Figure 1 Schematic diagram of plane elastic problem with circular cutouts and mesh used in the HFS-FEM

$$\left.\begin{aligned}&[\mathbf{L}]\{\boldsymbol{\sigma}\}+\{\bar{\mathbf{b}}\}=\{\mathbf{0}\}\\&\{\boldsymbol{\varepsilon}\}=[\mathbf{L}]^{\mathrm{T}}\{\mathbf{u}\}\\&\{\boldsymbol{\sigma}\}=[\mathbf{D}]\{\boldsymbol{\varepsilon}\}\end{aligned}\right\}\quad \text{in } \Omega \tag{1}$$

where $\{\boldsymbol{\sigma}\}=\{\sigma_{11}\quad \sigma_{22}\quad \sigma_{12}\}^{\mathrm{T}}$ and $\{\boldsymbol{\varepsilon}\}=\{\varepsilon_{11}\quad \varepsilon_{22}\quad \gamma_{12}\}^{\mathrm{T}}$ denote stress and strain vectors, respectively, $\{\bar{\mathbf{b}}\}=\{\bar{b}_1\quad \bar{b}_2\}^{\mathrm{T}}$ body force vector, $\{\mathbf{u}\}=\{u_1\quad u_2\}^{\mathrm{T}}$ displacement vector, and

$$\mathbf{L}=\begin{bmatrix}\partial_{,1} & 0 & \partial_{,2}\\ 0 & \partial_{,2} & \partial_{,1}\end{bmatrix} \tag{2}$$

the differential matrix, in which a comma denotes partial differentiation, i.e. $\partial_{,i}=\partial/\partial X_i$, and X_i $(i=1,2)$ are the global Cartesian coordinates. The stress-strain matrix is given by

$$\mathbf{D}=\frac{E^*}{1-\nu^{*2}}\begin{bmatrix}1 & \nu^* & 0\\ \nu^* & 1 & 0\\ 0 & 0 & \frac{1-\nu^*}{2}\end{bmatrix} \tag{3}$$

with $E^*=E$, $\nu^*=\nu$ for a plane stress problem and $E^*=E/(1-\nu^2)$, $\nu^*=\nu/(1-\nu)$ for a plane strain problem. E and ν denote respectively the elastic modulus and the Poisson's ratio.

Besides, following boundary displacement and traction conditions should be complemented to keep the system complete

$$\left.\begin{aligned}&\{\mathbf{u}\}=\{\bar{\mathbf{u}}\} && \text{on } \Gamma_u\\&\{\mathbf{s}\}=[\mathbf{A}]\{\boldsymbol{\sigma}\}=\{\bar{\mathbf{s}}\} && \text{on } \Gamma_s\end{aligned}\right\} \tag{4}$$

where the overbar represents a given value, and

$$[\mathbf{A}]=\begin{bmatrix}n_1 & 0 & n_2\\ 0 & n_2 & n_1\end{bmatrix} \tag{5}$$

with n_i representing the ith component of the unit outward normal to the boundary $\Gamma=\Gamma_u+\Gamma_s$.

Rearranging Eq. (1) leads to the following Cauchy-Navier equations in terms of displacements

$$[\mathbf{L}][\mathbf{D}][\mathbf{L}]^{\mathrm{T}}\{\mathbf{u}\}+\{\bar{\mathbf{b}}\}=\{\mathbf{0}\} \tag{6}$$

2. Fundamental solutions

For plane elastic problems involving holes, it is convenient to express the fundamental solutions in terms of complex variables. In plane elastic theory, all components of elastic fields including the stresses $\sigma_{11},\sigma_{22},\sigma_{12}$, the displacements u_1,u_2 and the resultant forces P_1,P_2 along a curve can be expressed in terms of two complex analytic functions $\phi(z)$ and $\psi(z)$ as[110]

$$\begin{cases}2G(u_1+u_2\mathrm{I})=\kappa\phi(z)-z\overline{\phi'(z)}-\overline{\psi(z)}\\ \sigma_{11}+\sigma_{22}=4\,\mathrm{Re}[\phi'(z)]\\ \sigma_{22}-\sigma_{11}+2\sigma_{12}\mathrm{I}=2\{\bar{z}\phi''(z)+\psi'(z)\}\\ P_1+P_2\mathrm{I}=2\mathrm{I}\{\phi(z)+z\overline{\phi'(z)}+\overline{\psi(z)}\}\end{cases} \tag{7}$$

where $G=E/2/(1+\nu)$, $\kappa=(3-\nu)/(1+\nu)$ for plane stress and $\kappa = 3-4\nu$ for plane strain, $z = x_1 + x_2 \mathrm{I}$ is the complex coordinate in the z−plane with $\mathrm{I} = \sqrt{-1}$, the overbar denotes complex conjugation, Re denotes the real part of the function and prime denotes differentiation with respect to the argument z.

A point force in an infinite plane

If a concentrated force $F = F_1 + F_2 \mathrm{I}$ is located at the point $z_0 = x_1^s + x_2^s \mathrm{I}$ in the infinite plane, the complex functions can be written as[110]

$$\begin{cases} \phi(z) = M \ln(z - z_0) \\ \psi(z) = N \ln(z - z_0) - M \dfrac{\bar{z}_0}{z - z_0} \end{cases} \tag{8}$$

where

$$M = -\frac{F}{2\pi(1+\kappa)}, \quad N = -\kappa \bar{M}$$

Obviously, the complex functions in Eq. (8) are singular at the point z_0, which can be taken as the basis for constructing more complex fundamental solutions.

By substituting Eq. (8) into Eq. (7), the classical formation of the Kelvin solution can be obtained. For example, for plane strain problems, if $u_{li}^*(z, z_0)$ and $\sigma_{lij}^*(z, z_0)$ are the induced displacements and stresses at z due to l-direction unit force at z_0, we have[36]

Making use of the new variables defined by Eq (8), the Laplace operator in Eq (3) becomes

$$\begin{aligned} u_{li}^* &= \frac{1}{8\pi G(1-\nu)} \left[(3-4\nu)\delta_{li} \ln\frac{1}{r} + r_{,l} r_{,i} \right] \\ \sigma_{lij}^* &= \frac{1}{4\pi(1-\nu) r} \left[(1-2\nu)\left(r_{,l}\delta_{ij} - r_{,j}\delta_{il} - r_{,i}\delta_{jl} \right) - 2 r_{,i} r_{,j} r_{,l} \right] \end{aligned} \tag{9}$$

where r stands for the distance between z and z_0.

A point force in an infinite plane with circular hole

Consider a point force $F = F_1 + F_2 \mathrm{I}$ at z_0 in an infinite plane with a centered circular hole of radius a. Using the complex variable formalism above, the fundamental solution sought can be expressed in the form

$$\begin{cases} \phi(z) = \phi_s(z) + \phi_r(z) \\ \psi(z) = \psi_s(z) + \psi_r(z) \end{cases} \tag{10}$$

where where ϕ_s and ψ_s are the singular terms for the infinite homogeneous body, which is the Kelvin's solution expressed in terms of complex variable listed above, and ϕ_r and ψ_r are regular terms to be determined so that the resultant tractions on the surface of the circular hole become zero. Furthermore, the vanishing stress conditions at infinity should also be satisfied.

Using the analytical continuation approach, the regular terms (also called imaging terms) can be obtained as

$$\begin{cases} \phi_r(z, z_0^*) = -z\overline{\phi_s'(z^*, z_0)} - \overline{\psi_s(z^*, z_0)} \\ \psi_r(z, z_0^*) = -\overline{\phi_s(z^*, z_0)} - \bar{z}^* \phi_r'(z, z_0^*) \end{cases} \tag{11}$$

where $z^* = a^2 / \bar{z}$, $z_0^* = a^2 / \bar{z}_0$.

Substituting the known singular terms and retaining the main parts of Eq. (11) gives the following solutions:

$$\begin{cases} \phi_r(z, z_0) = -\bar{N} \ln(\dfrac{z - z_0^*}{z}) - \bar{M} \dfrac{z_0 - z_0^*}{z - z_0^*} \dfrac{z_0^*}{\bar{z}_0} \\ \psi_r(z, z_0) = -\bar{M} \ln(\dfrac{z - z_0^*}{z}) + \bar{N} \dfrac{a^2}{z - z_0^*} \dfrac{1}{z} \\ \qquad - \bar{N} \dfrac{a^2}{z^2} - \bar{M} \dfrac{z_0^{*2}(z_0 - z_0^*)}{z(z - z_0^*)^2} + M \dfrac{\bar{z}_0^*}{z} \end{cases} \tag{12}$$

Having determined the two complex functions, the related displacement and stress solutions can be obtained using Eq. (7).

3. Hybrid FE Implementation

In this section, the procedure for developing a hybrid finite element model with the fundamental solutions as the interior trial functions is described for solving the boundary value problem (BVP) defined by Eqs. (1), (4), and Eq. (13) below.

As in the hybrid Trefftz FEM, the main aim of the proposed approach is to establish a hybrid finite element formulation whereby intra-element continuity is enforced on nonconforming internal displacement fields formed by a linear combination of fundamental solutions at source points outside the element domain under consideration, while auxiliary frame displacement fields are independently defined on the element boundary to enforce field continuity across inter-element boundaries. But unlike the hybrid Trefftz FEM, the intra-element fields in the HFS-FEM are constructed based on the fundamental solutions, rather than a truncated T-complete function set. Subsequently, a variational functional associated with the new displacement trial functions inside the element and displacements on the element boundary is required to generate the related stiffness matrix equation. As the solution domain is divided into a number of elements denoted by Ω_e with the element boundary Γ_e, the following inter-element continuity related to displacements and tractions is usually required on the common boundary Γ_{Ief} between any two adjacent elements 'e' and 'f' (see Figure 2):

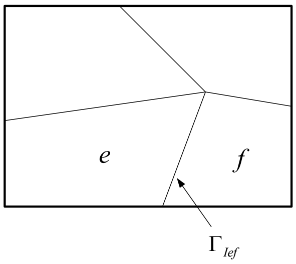

Figure 2. Illustration of continuity between two adjacent elements 'e' and 'f' in the proposed hybrid FE approach.

$$\left.\begin{array}{l}\{\mathbf{u}_e\}=\{\mathbf{u}_f\}\\ \{\mathbf{s}_e\}+\{\mathbf{s}_f\}=\{\mathbf{0}\}\end{array}\right\} \quad \text{on } \Gamma_e\cap\Gamma_f \tag{13}$$

Non-conforming intra-element fields

In the absence of body forces, and motivated by the method of fundamental solution (MFS) to remove the singularity of the fundamental solution, for a particular element shown in Figure 3, say element e, which occupies the sub-domain Ω_e, we first assume that the field variable defined in the element domain is approximated by a linear combination of fundamental solutions centered at different source points (see Figure 3) as

$$\{\mathbf{u}_e\}=\sum_{j=1}^{n_s}\begin{bmatrix}u_{11}^*(\mathbf{x},\mathbf{y}_j) & u_{21}^*(\mathbf{x},\mathbf{y}_j)\\ u_{12}^*(\mathbf{x},\mathbf{y}_j) & u_{22}^*(\mathbf{x},\mathbf{y}_j)\end{bmatrix}\begin{Bmatrix}c_{1j}\\ c_{2j}\end{Bmatrix}=[\mathbf{N}]\{\mathbf{c}_e\} \quad (\forall\mathbf{x}\in\Omega_e,\mathbf{y}_j\notin\Omega_e) \tag{14}$$

where n_s is the number of virtual sources outside the element domain, $\{\mathbf{c}_e\}=\begin{bmatrix}c_{11} & c_{21} & \cdots & \cdots & c_{2n_s}\end{bmatrix}^{\mathrm{T}}$ is an unknown coefficient vector (not nodal displacements), and the coefficient matrix

$$[\mathbf{N}]=\begin{bmatrix}u_{11}^*(\mathbf{x},\mathbf{y}_1) & u_{21}^*(\mathbf{x},\mathbf{y}_1) & \cdots & \cdots(\mathbf{x},\mathbf{y}_{n_s}) & u_{21}^*(\mathbf{x},\mathbf{y}_{n_s})\\ u_{12}^*(\mathbf{x},\mathbf{y}_1) & u_{22}^*(\mathbf{x},\mathbf{y}_1) & \cdots & \cdots(\mathbf{x},\mathbf{y}_{n_s}) & u_{22}^*(\mathbf{x},\mathbf{y}_{n_s})\end{bmatrix} \tag{15}$$

where $\mathbf{x}$ and $\mathbf{y}_i$ are the field point and source point defined in the local coordinate system (x_1,x_2):

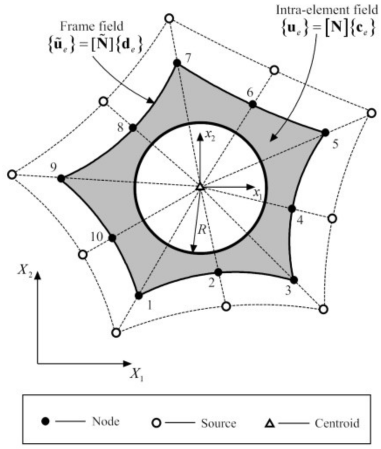

Figure 1. Intra-element fields and frame fields in a particular element in the HFS-FEM

Subsequently, differentiating Eq. (14) and substituting it into Eq. (1) yields the corresponding stress fields

By invoking the divergence theorem

$$\{\boldsymbol{\sigma}_e\}=[\mathbf{T}]\{\mathbf{c}_e\} \tag{16}$$

with

$$[\mathbf{T}]=\begin{bmatrix}\sigma_{111}^*(\mathbf{x},\mathbf{y}_1) & \sigma_{211}^*(\mathbf{x},\mathbf{y}_1) & \cdots & \cdots(\mathbf{x},\mathbf{y}_{n_s}) & \sigma_{211}^*(\mathbf{x},\mathbf{y}_{n_s})\\ \sigma_{122}^*(\mathbf{x},\mathbf{y}_1) & \sigma_{222}^*(\mathbf{x},\mathbf{y}_1) & \cdots & \cdots(\mathbf{x},\mathbf{y}_{n_s}) & \sigma_{222}^*(\mathbf{x},\mathbf{y}_{n_s})\\ \sigma_{112}^*(\mathbf{x},\mathbf{y}_1) & \sigma_{212}^*(\mathbf{x},\mathbf{y}_1) & \cdots & \cdots(\mathbf{x},\mathbf{y}_{n_s}) & \sigma_{212}^*(\mathbf{x},\mathbf{y}_{n_s})\end{bmatrix}$$

Furthermore, the element boundary traction vector $\{\mathbf{s}_e\}$ is evaluated by

$$\{\mathbf{s}_e\}=[\mathbf{Q}]\{\mathbf{c}_e\}=[\mathbf{A}][\mathbf{T}]\{\mathbf{c}_e\} \tag{17}$$

Auxiliary conforming frame fields

In order to enforce conformity on the displacement vector $\{\mathbf{u}\}$ along the inter-element boundary, for instance $\{\mathbf{u}_e\}=\{\mathbf{u}_f\}$ on $\Gamma_e\cap\Gamma_f$, of any two neighboring elements e and f, auxiliary inter-element frame fields $\{\tilde{\mathbf{u}}_e\}$ are assumed in terms of the nodal degrees of freedom (DOF), $\{\mathbf{d}_e\}$, as used in the conventional FEM. For example, for the element shown in Figure 3 containing 10 nodes, the frame fields $\{\tilde{\mathbf{u}}_e\}$ over the second edge consisting of nodes 3, 4, and 5 are written as

$$\{\tilde{\mathbf{u}}_e\}=[\tilde{\mathbf{N}}]\{\mathbf{d}_e\} \tag{18}$$

in which the shape function matrix $[\tilde{\mathbf{N}}]$ and the nodal vector $\{\mathbf{d}_e\}$ are given by

$$[\tilde{N}_e] = \begin{bmatrix} 0 & 0 & \cdots & & \cdots \\ 0 & 0 & \cdots & & \cdots \end{bmatrix}$$

$$\{\mathbf{d}_e\} = \{u_1^1 \quad u_2^1 \;\vdots\; \cdots \quad \cdots\}^{\mathrm{T}}$$

and $\tilde{N}_i$ ($i = 1,2,3$) stands for shape functions in terms of the natural coordinate ξ defined in Figure 4, u_i^k $(i = 1,2)$ denotes the nodal displacement at nodal k.

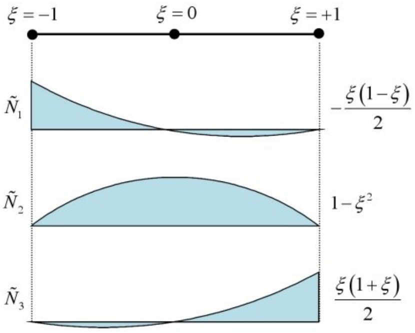

Figure 2. Typical quadratic interpolation for the frame fields

B. Special elliptical hole element

1. Element Formulation

The HT FE model used here is based on simultaneous use of two independent displacement fields (Figure 3)

(a) a non-conforming 'Trefftz' field

$$\mathbf{u}_e = \breve{\mathbf{u}}_e + \sum_{j=1}^{m} \mathbf{N}_{ej} c_{ej} = \breve{\mathbf{u}}_e + \mathbf{N}_e \mathbf{c}_e \tag{19}$$

where c_{ej} stands for undetermined coefficients and $\breve{\mathbf{u}}_e$ and $\mathbf{N}_{ej}$ are the particular and homogeneous solutions to the governing differential equations.

(b) an exactly and minimally conforming auxiliary frame field

$$\tilde{\mathbf{u}}_e = \tilde{\mathbf{N}}_e \mathbf{d}_e \text{ on } \Gamma_e \tag{20}$$

being independently assumed along the element boundary in terms of nodal degrees of freedom $\mathbf{d}_e$, where $\Gamma_e = \Gamma_{eu} \cup \Gamma_{et} \cup \Gamma_{eI}$, while $\Gamma_{eu} = \Gamma_u \cap \Gamma_e$, $\Gamma_{et} = \Gamma_t \cap \Gamma_e$, and Γ_{eI} is the inter-element boundary, $\tilde{\mathbf{N}}_e$ are the shape functions (frame functions) defined in the customary way as in conventional FEM. The tilde above a symbol in Eq. (20) allows the two fields to be distinguished.

The corresponding stress field

$$\boldsymbol{\sigma}_e = \breve{\boldsymbol{\sigma}}_e + \sum_{j=1}^{m} \mathbf{T}_{ej} c_{ej} = \breve{\boldsymbol{\sigma}}_e + \mathbf{T}_e \mathbf{c}_e \tag{21}$$

as well as the boundary tractions

$$\mathbf{t}_e = \breve{\mathbf{t}}_e + \sum_{j=1}^{m} \mathbf{Q}_{ej} c_{ej} = \breve{\mathbf{t}}_e + \mathbf{Q}_e \mathbf{c}_e \tag{22}$$

can be readily deduced from $\boldsymbol{\sigma}_e = \mathbf{D}\mathbf{L}^{\mathrm{T}}\mathbf{u}_e$ and $\mathbf{t}_e = \mathbf{A}\boldsymbol{\sigma}_e$ respectively, where $\mathbf{L}$ is the differential operator matrix, $\mathbf{D}$ contains elastic constants and $\mathbf{A}$ contains components of a unit normal to the element boundary Γ_e.

The HT FE formulation for 2D elastic problems may be obtained by means of the following modified variational principle

$$\Pi_m = \Pi_c - \sum_e \left[\int_{\Gamma_{et}} \left(\mathbf{t}_e - \bar{\mathbf{t}}_e\right)^{\mathrm{T}} \tilde{\mathbf{u}}_e \,\mathrm{d}\Gamma + \int_{\Gamma_{eI}} \mathbf{t}_e^{\mathrm{T}} \tilde{\mathbf{u}}_e \,\mathrm{d}\Gamma \right] \tag{23}$$

where Π_c is the total complementary energy, the overhead bar is used to designate specified values.

Applying the stationary condition to Eq. (23) straightforwardly leads to the symmetric element stiffness equation

$$\mathbf{K}_e \mathbf{d}_e = \mathbf{P}_e \tag{24}$$

where

$$\mathbf{K}_e = \mathbf{G}_e^{\mathrm{T}} \mathbf{H}_e^{-1} \mathbf{G}_e \tag{25}$$

$$\mathbf{P}_e = \mathbf{G}_e^{\mathrm{T}} \mathbf{H}_e \mathbf{h}_e - \mathbf{g}_e \tag{26}$$

Here the auxiliary matrices $\mathbf{H}_e$, $\mathbf{G}_e$, $\mathbf{h}_e$ and $\mathbf{g}_e$ are explicitly expressed as

$$\mathbf{H}_e = \int_{\Gamma_e} \mathbf{Q}_e^{\mathrm{T}} \mathbf{N}_e \,\mathrm{d}\Gamma = \int_{\Gamma_e} \mathbf{N}_e^{\mathrm{T}} \mathbf{Q}_e \,\mathrm{d}\Gamma \tag{27}$$

$$\mathbf{G}_e = \int_{\Gamma_e} \mathbf{Q}_e^{\mathrm{T}} \tilde{\mathbf{N}}_e \,\mathrm{d}\Gamma \tag{28}$$

$$\mathbf{h}_e = \frac{1}{2} \int_{\Gamma_e} \left(\mathbf{N}_e^{\mathrm{T}} \breve{\mathbf{t}} + \mathbf{Q}_e^{\mathrm{T}} \breve{\mathbf{u}}_e \right) \mathrm{d}\Gamma + \frac{1}{2} \iint_{\Omega_e} \mathbf{N}_e^{\mathrm{T}} \bar{\mathbf{b}}_e \,\mathrm{d}\Omega \tag{29}$$

$$\mathbf{g}_e = \int_{\Gamma_e} \tilde{\mathbf{N}}_e^{\mathrm{T}} \breve{\mathbf{t}}_e \,\mathrm{d}\Gamma - \int_{\Gamma_{et}} \tilde{\mathbf{N}}_e^{\mathrm{T}} \bar{\mathbf{t}}_e \,\mathrm{d}\Gamma \tag{30}$$

in which $\bar{\mathbf{b}}_e$ stand for the body forces.

2. Special Trefftz functions

A key step in constructing an accurate special finite element for a region with a hole is to find a special set of trail functions which reflect the local stress concentration characteristics. To achieve this, the

Muskhelishvili's complex variable formulation is utilized herein (see Figure 5). The number of Trefftz functions m for elliptical hole elements is suggested here to be equal to the number of elemental degrees of freedom. The derivation of special Trefftz function can be carried out by using following expressions of displacements and stresses.

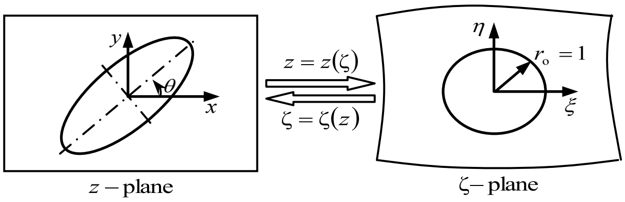

Figure 5. Conformal mapping for constructing special hole element

$$2G(u+iv)=\kappa\phi(z)-z\overline{\dot{\phi}}(z)-\overline{\psi}(z) \quad (31)$$

$$\sigma_{xx}+i\sigma_{xy}=\dot{\phi}(z)+\overline{\dot{\phi}}(z)-z\overline{\ddot{\phi}}(z)-\overline{\dot{\psi}}(z) \quad (32)$$

$$\sigma_{yy}-i\sigma_{xy}=\dot{\phi}(z)+\overline{\dot{\phi}}(z)+z\overline{\ddot{\phi}}(z)+\overline{\dot{\psi}}(z) \quad (33)$$

where $z=x+iy$, $i=\sqrt{-1}$, $\phi(z)$ and $\psi(z)$ are two analytical functions, $G=E/2(1+\mu)$, $\kappa=(3-\mu)/(1+\mu)$, E and μ are, respectively, Young's modulus and Poisson's ratio, $(\dot{\ })$ denotes differentiation with respect to z and $\overline{(\ )}$ represents complex conjugate. The boundary conditions can be given in the complex form as

$$\kappa\phi(z)-z\overline{\dot{\phi}}(z)-\overline{\psi}(z)=2G(\bar{u}+i\bar{v}) \quad \text{on}\,\Gamma_u \quad (34)$$

$$\phi(z)+z\overline{\dot{\phi}}(z)+\overline{\psi}(z)=i\int(\bar{t}_x+i\bar{t}_y)\,\mathrm{d}\Gamma \quad \text{on}\,\Gamma_t \quad (35)$$

It is tedious to treat structures with holes in arbitrary direction. To bypass this difficulty, a rotated mapping function

$$\wp(\theta)=e^{i\theta} \quad (36)$$

is introduced into the horizontal conformal transformation as (see Figure 5)

$$z=f(\zeta)=\wp(\theta)c\left(\zeta+m\zeta^{-1}\right)=ce^{i\theta}\left(\zeta+m\zeta^{-1}\right) \quad (37)$$

where $c=(a+b)/2$, $m=(a-b)/(a+b)$, a and b are, respectively, the semi-major axis and semi-minor axis, θ is the angle between the semi-major axis and x axis.

Substituting the inverse transformation

$$\zeta=f^{-1}(z)=\frac{1}{2ce^{i\theta}}\left(z\pm\sqrt{z^2+4c^2me^{i2\theta}}\right) \quad (38)$$

into Eqs. (31)-(33) produces the displacements and stresses in the ξ-plane as:

$$2G\left(u_x+iu_y\right)=\kappa\phi-f\frac{\overline{\dot{\phi}}}{\overline{\dot{f}}}-\overline{\psi} \quad (39)$$

$$\sigma_{xx}-i\tau_{xy}=\frac{\dot{\phi}}{\dot{f}}+\frac{\overline{\dot{\phi}}}{\overline{\dot{f}}}-\frac{\bar{f}\left(\dot{f}\ddot{\phi}-\ddot{f}\dot{\phi}\right)}{\dot{f}^3}-\frac{\dot{\psi}}{\dot{f}} \quad (40)$$

$$\sigma_{yy}-i\tau_{xy}=\frac{\dot{\phi}}{\dot{f}}+\frac{\overline{\dot{\phi}}}{\overline{\dot{f}}}+\frac{\bar{f}\left(\dot{f}\ddot{\phi}-\ddot{f}\dot{\phi}\right)}{\dot{f}^3}+\frac{\dot{\psi}}{\dot{f}} \quad (41)$$

Here, the sign in Eq. (38) is chosen in the similar way with Ref [110].

The transformed boundary conditions along the hole surface can be expressed as

$$\psi(\zeta)=\kappa\bar{\phi}-\bar{f}\frac{\dot{\phi}}{\dot{f}}-2G\left(\overline{u+iv}\right) \quad \text{on } \Gamma_u' \quad (42)$$

$$\psi(\zeta)=-\bar{\phi}-\bar{f}\frac{\dot{\phi}}{\dot{f}}-i\int\overline{\left(t_x+it_y\right)}\,\mathrm{d}\Gamma \quad \text{on } \Gamma_t' \quad (43)$$

In general, it is impossible to find a closed form formulation for $\phi(\xi)$ and $\psi(\xi)$ for arbitrary geometry and boundary conditions. By expanding the two holomorphic functions in the general expressions of elasticity solutions into two complex Laurent series respectively we have

$$\phi(\zeta)=\sum_{j=-N}^{M}c_j\zeta^j \quad (44)$$

$$\psi(\zeta)=-\sum_{j=-N}^{M}\left[\bar{c}_j\zeta^{-j}+c_j j\frac{\zeta^{j-2}+m\zeta^j}{e^{i2\theta}\left(1-m\zeta^{-2}\right)}\right] \quad (45)$$

where $c_j=a_j+ib_j$ are complex coefficients, M and N are the upper and lower limits of the Laurent series and M is generally set to be N for symmetry, Eq. (45) is obtained according to the traction-free condition along the hole boundary. Therefore, the displacement and stress fields are given in the following form

$$2G\left(u_x+iu_y\right)=\sum_{j=-N}^{M}\left[\left(\varsigma_1-\varsigma_2\right)a_j+i\left(\varsigma_1+\varsigma_2\right)b_j\right] \quad (46)$$

$$\begin{aligned}\sigma_{xx}-i\tau_{xy}=\sum_{j=-N}^{M}&\left[\chi_1+\chi_2-\chi_3-\chi_4+\chi_5\right]a_j\\&+\left[\chi_1-\chi_2-\chi_3+\chi_4+\chi_5\right]b_j\end{aligned} \quad (47)$$

$$\begin{aligned}\sigma_{yy}+i\tau_{xy}=\sum_{j=-N}^{M}&\left[\chi_1+\chi_2+\chi_3+\chi_4-\chi_5\right]a_j\\&+\left[\chi_1-\chi_2+\chi_3-\chi_4-\chi_5\right]b_j\end{aligned} \quad (48)$$

where

$$\varsigma_1=\kappa\zeta^j+\bar{\zeta}^{-j} \quad (49)$$

$$\varsigma_2=\frac{je^{i2\theta}\bar{\zeta}^{j-1}\left[\zeta-\bar{\zeta}^{-1}+m\left(\zeta^{-1}-\bar{\zeta}\right)\right]}{1-m\bar{\zeta}^{-2}} \quad (50)$$

$$\chi_1 = \frac{j\zeta^{j-1}}{ce^{i\theta}\left(1 - m\zeta^{-2}\right)} \tag{51}$$

$$\chi_2 = \frac{je^{i\theta}\bar{\zeta}^{j-1}}{c\left(1 - m\bar{\zeta}^{-2}\right)} \tag{52}$$

$$\chi_3 = \frac{j\left(\bar{\zeta} + m\bar{\zeta}^{-1}\right)\left[\left(j-1\right)\zeta^{j-2} + \left(j+1\right)\zeta^{j-4}\right]}{ce^{i3\theta}\left(1 - m\zeta^{-2}\right)^3} \tag{53}$$

$$\chi_4 = \frac{j\zeta^{-j-1}}{ce^{i\theta}\left(1 - m\zeta^{-2}\right)} \tag{54}$$

$$\chi_5 = \frac{j\left[\left(\left(j-2\right) - m^2\left(j+2\right)\right)\zeta^{j-3} - mj\zeta^{j-5} + mj\zeta^{j-1}\right]}{ce^{i3\theta}\left(1 - m\zeta^{-2}\right)^3} \tag{55}$$

From Eqs. (39)-(41) the special Trefftz functions $\mathbf{N}_e$ and $\mathbf{T}_e$ may be written as follows

$$\mathbf{N}_e = \frac{1}{2G}\begin{bmatrix} \mathrm{Re}U_{-N} & \cdots & \mathrm{Re}U_M & \mathrm{Re}U_{M+N+1} & \cdots & \mathrm{Re}U_{2(M+N)} \\ \mathrm{Im}U_{-N} & \cdots & \mathrm{Im}U_M & \mathrm{Im}U_{M+N+1} & \cdots & \mathrm{Im}U_{2(M+N)} \end{bmatrix}$$

(56)

$$\mathbf{T}_e = \begin{bmatrix} \mathrm{Re}S_{1,-N} & \cdots & \mathrm{Re}S_{1,M+N} & \mathrm{Re}S_{1,M+N+1} & \cdots & \mathrm{Re}S_{1,2(M+N)} \\ \mathrm{Re}S_{2,-N} & \cdots & \mathrm{Re}S_{2,M+N} & \mathrm{Re}S_{2,M+N+1} & \cdots & \mathrm{Re}S_{2,2(M+N)} \\ \mathrm{Im}S_{3,-N} & \cdots & \mathrm{Im}S_{3,M+N} & \mathrm{Im}S_{3,M+N+1} & \cdots & \mathrm{Im}S_{3,2(M+N)} \end{bmatrix} \tag{57}$$

where

$$U_j = \varsigma_1 - \varsigma_2 \tag{58}$$

$$U_{M+N+j} = i\left(\varsigma_1 + \varsigma_2\right) \tag{59}$$

$$S_{1,j} = \chi_1 + \chi_2 - \chi_3 - \chi_4 + \chi_5 \tag{60}$$

$$S_{1,M+N+j} = \chi_1 - \chi_2 - \chi_3 + \chi_4 + \chi_5 \tag{61}$$

$$S_{2,j} = \chi_1 + \chi_2 + \chi_3 + \chi_4 - \chi_5 \tag{62}$$

$$S_{2,M+N+j} = \chi_1 - \chi_2 + \chi_3 - \chi_4 - \chi_5 \tag{63}$$

$$S_{3,j} = \chi_3 + \chi_4 - \chi_5 \tag{64}$$

$$S_{3,M+N+j} = \chi_3 - \chi_4 - \chi_5 \tag{65}$$

Frame functions

Here we use the 16- and 32-node hole elements (RHOL16 and RHOL32 for short), as shown in Figure 6, to conduct the contact analysis.

For each side of RHOL16 element, the frame functions are of the form

$$\begin{cases} \widetilde{N}_1 = \frac{2}{3}\left(\tau^2 - \frac{1}{4}\right)\tau\left(\tau - 1\right) \\ \widetilde{N}_2 = -\frac{8}{3}\left(\tau^2 - 1\right)\tau\left(\tau - \frac{1}{2}\right) \\ \widetilde{N}_3 = 4\left(\tau^2 - 1\right)\left(\tau^2 - \frac{1}{4}\right) \\ \widetilde{N}_4 = -\frac{8}{3}\left(\tau^2 - 1\right)\tau\left(\tau + \frac{1}{2}\right) \\ \widetilde{N}_5 = \frac{2}{3}\left(\tau^2 - \frac{1}{4}\right)\tau\left(\tau + 1\right) \end{cases} \tag{66}$$

Analogously, for each side of RHOL32 element, the frame functions may be written as

$$\begin{cases} \widetilde{N}_1 = \frac{512}{315}\left(\tau^2 - \frac{9}{16}\right)\left(\tau^2 - \frac{1}{4}\right)\left(\tau^2 - \frac{1}{16}\right)\tau\left(\tau - 1\right) \\ \widetilde{N}_2 = -\frac{4096}{315}\left(\tau^2 - 1\right)\left(\tau^2 - \frac{1}{4}\right)\left(\tau^2 - \frac{1}{16}\right)\tau\left(\tau - \frac{3}{4}\right) \\ \widetilde{N}_3 = \frac{2048}{45}\left(\tau^2 - 1\right)\left(\tau^2 - \frac{9}{16}\right)\left(\tau^2 - \frac{1}{16}\right)\tau\left(\tau - \frac{1}{2}\right) \\ \widetilde{N}_4 = -\frac{4096}{45}\left(\tau^2 - 1\right)\left(\tau^2 - \frac{9}{16}\right)\left(\tau^2 - \frac{1}{4}\right)\tau\left(\tau - \frac{1}{4}\right) \\ \widetilde{N}_5 = \frac{1024}{9}\left(\tau^2 - 1\right)\left(\tau^2 - \frac{9}{16}\right)\left(\tau^2 - \frac{1}{4}\right)\left(\tau - \frac{1}{16}\right) \\ \widetilde{N}_6 = -\frac{4096}{45}\left(\tau^2 - 1\right)\left(\tau^2 - \frac{9}{16}\right)\left(\tau^2 - \frac{1}{4}\right)\tau\left(\tau + \frac{1}{4}\right) \\ \widetilde{N}_7 = \frac{2048}{45}\left(\tau^2 - 1\right)\left(\tau^2 - \frac{9}{16}\right)\left(\tau^2 - \frac{1}{16}\right)\tau\left(\tau + \frac{1}{2}\right) \\ \widetilde{N}_8 = -\frac{4096}{315}\left(\tau^2 - 1\right)\left(\tau^2 - \frac{1}{4}\right)\left(\tau^2 - \frac{1}{16}\right)\tau\left(\tau + \frac{3}{4}\right) \\ \widetilde{N}_9 = \frac{512}{315}\left(\tau^2 - \frac{9}{16}\right)\left(\tau^2 - \frac{1}{4}\right)\left(\tau^2 - \frac{1}{16}\right)\tau\left(\tau + 1\right) \end{cases}$$

(67)

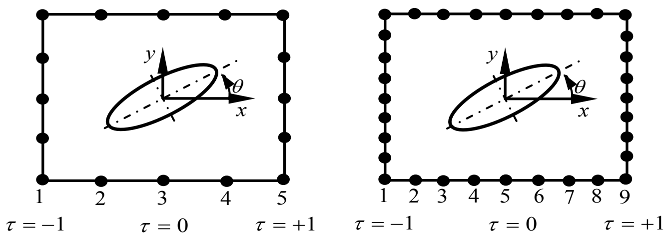

(a) RHOL16 (b) RHOL32

Figure 6. New special Trefftz hole element

C. Special elements for discontinuous loads

1. Basic equations of plane elasticity

In this section, the plane elasticity is briefly reviewed for establishing notation and formulation used in later sections. Let us consider a well-posed elastic problem in a domain denoted by Ω bounded by its boundary Γ. The corresponding partial differential governing equations and boundary conditions are given by

$$\left.\begin{aligned} &\sigma_{ij,j} + b_i = 0 \\ &\varepsilon_{ij} = \frac{1}{2}\left(u_{i,j} + u_{j,i}\right) \\ &\sigma_{ij} = \lambda\delta_{ij}\varepsilon_{kk} + 2\mu\varepsilon_{ij} \end{aligned}\right\} \quad \text{in } \Omega \tag{68}$$

and

$$\left.\begin{aligned} &u_i = \bar{u}_i && \text{on } \Gamma_u \\ &s_i = \sigma_{ij}n_j = \bar{s}_i && \text{on } \Gamma_s \end{aligned}\right\} \tag{69}$$

where σ_{ij} is the stress tensor, b_i is the body force component, a comma denotes partial differentiation and the Einstein summation convention over repeated indices is used. ε_{ij} denotes the elastic strain tensor, u_i is the displacement field component and δ_{ij} is Kronecker's delta, λ and μ are respectively the Lame elastic constants and usually can be expressed in terms of Young's modulus E and Poisson ratio ν as

$$\lambda = \frac{3-\kappa}{\kappa-1}\mu, \qquad \mu = \frac{E}{2(1+\nu)} \tag{70}$$

with $\kappa = 3-4\nu$ for plane strain state and $\kappa = (3-\nu)/(1+\nu)$ for plane stress state $\overline{u}_i$ and $\overline{s}_i$ are imposed boundary displacement and traction components, respectively, $\Gamma = \Gamma_u \cup \Gamma_q$ is the boundary of the solution domain Ω . n_i represents the i th component of outward normal vector to the boundary Γ .

Eq. (68) can be written in one equation as

$$\{\lambda+\mu\}u_{j,ji}(\mathbf{x}) + \mu u_{i,jj}(\mathbf{x}) + b_i = 0 \tag{71}$$

which is the classic Navier-Cauchy equations in terms of displacement fields.

When the body force becomes a unit concentrated force applied at point $\mathbf{x}^s$ in an infinite domain, the solutions of Eq. (71) is known as fundamental solutions or Green's functions.. This physical definition of fundamental solution can be used in the present hybrid finite element model to construct local solutions employed in the proposed special elements to effectively deal with internal discontinuous forces.

2. Local solutions of discontinuous loads

We focus on local solutions induced by internal point, line and patch loads, as displayed in Figure 7. All these internal loads can be regarded as generalized body forces from the view point of mechanics such that their effects can be represented by the fundamental solutions as follows.

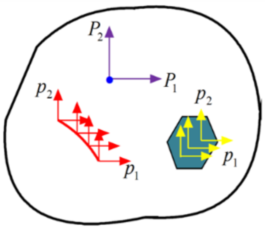

Figure 7. Sketch of plane elastic domain under internal discontinuous loads

Local solutions due to point loads

Let's consider a plane elastic problem in an infinite domain subjected to a pair of internal concentrated forces (P_1, P_2), as shown in Figure 8. In this case, the concentrated force can be regarded as the generalized body forces with intensity $P_i\delta(\mathbf{x}-\mathbf{x}^s)$ $(i=1,2)$ at the point $\mathbf{x}^s = (x_1^s, x_2^s)$, thus the Navier-Cauchy equation (71) can be written as

$$\{\lambda+\mu\}u_{j,ji}(\mathbf{x}) + \mu u_{i,jj}(\mathbf{x}) + P_i\delta(\mathbf{x}-\mathbf{x}^s) = 0 \tag{72}$$

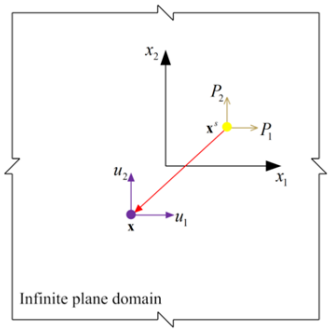

Figure 8. Concentrated forces in an infinite plane

Using the physical definition of fundamental solutions, the general solutions of Eq. (72) at any point $\mathbf{x} = (x_1, x_2)$ can be expressed as

$$u_i(\mathbf{x},\mathbf{x}^s) = U_{li}^*(\mathbf{x},\mathbf{x}^s)P_l \tag{73}$$

in which the kernel functions

$$U_{li}^*(\mathbf{x},\mathbf{x}^s) = \frac{1}{2\pi\mu(1+\kappa)}\left\{-\kappa\delta_{li}\ln r + \frac{r_i r_l}{r^2}\right\} \tag{74}$$

are the fundamental solutions of the problems. In Eq.(74), r is the distance between the points $\mathbf{x}$ and $\mathbf{x}^s$, i.e.

$$r = r_i r_i \quad \text{with } r_i = x_i - x_i^s \tag{75}$$

The substitution of Eq. (73) into the strain-displacement relation, and then into the constitutive equation given in Eq. (68) yield the following local stress fields induced by the imposed point loads (P_1, P_2)

$$\sigma_{ij}(\mathbf{x},\mathbf{x}^s) = S_{lij}^*(\mathbf{x},\mathbf{x}^s)P_l \tag{76}$$

with the stress fundamental solutions in the form as

$$S_{lij}^*(\mathbf{x},\mathbf{x}^s) = \frac{1}{2\pi(1+\kappa)}\left\{\frac{(1-\kappa)(\delta_{lj}r_i + \delta_{li}r_j - \delta_{ij}r_l)}{r^2} - \frac{4r_i r_j r_l}{r^4}\right\} \tag{77}$$

Local solutions due to line loads

For the case of arbitrarily distributed line loads as shown in Figure 9 with distributed load intensity p_1

and p_2 respectively parallel to x_1 and x_2 axis, the resultant forces on the differential element of arc length $\mathrm{d}L$ are given by

$$\mathrm{d}\mathbf{P} = \left\{ p_1(\mathbf{x}^s) \quad p_2(\mathbf{x}^s) \right\}^{\mathrm{T}} \delta(\mathbf{x},\mathbf{x}^s)\mathrm{d}L \tag{78}$$

which leads to the generalized boy forces as

$$\mathbf{b}(\mathbf{x}) = \int_{L_{AB}} \left\{ p_1(\mathbf{x}^s) \quad p_2(\mathbf{x}^s) \right\}^{\mathrm{T}} \delta(\mathbf{x},\mathbf{x}^s)\mathrm{d}L \tag{79}$$

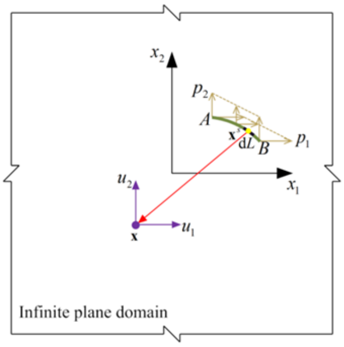

Figure 9. Effect of local line loads in an infinite plane

Hence, the induced displacement, strain and stress fields can be obtained by integrating the point-load solutions given in Eqs. (73)-(76) along the curved line segment L_{AB} and this leads to the following line integrals with respect to arc length along the curve L_{AB}

$$u_i(\mathbf{x}) = \int_{L_{AB}} U_{li}^*(\mathbf{x},\mathbf{x}^s)\, p_l(\mathbf{x}^s)\mathrm{d}L \tag{80}$$

$$\sigma_{ij}(\mathbf{x}) = \int_{L_{AB}} S_{lij}^*(\mathbf{x},\mathbf{x}^s)\, p_l(\mathbf{x}^s)\mathrm{d}L \tag{81}$$

If the smooth curve L_{AB} can be expressed in the form

$$x_2^s = f(x_1^s) \qquad \text{for } a \le x_1^s \le b \tag{82}$$

then the differential element of arc length dL can be written as

$$\mathrm{d}L = \sqrt{(\mathrm{d}x_1^s)^2 + (\mathrm{d}x_2^s)^2} = \Lambda(\mathbf{x}^s)\mathrm{d}x_1^s \tag{83}$$

where

$$\Lambda(\mathbf{x}^s) = \sqrt{1 + \left(\frac{\mathrm{d}f}{\mathrm{d}x_1^s}\right)^2} \tag{84}$$

Consequently, the line integrals above can be converted into general integrals in terms of single variable x_1

$$u_i(\mathbf{x}) = \int_a^b \left\{ U_{li}^*(\mathbf{x},\mathbf{x}^s)\, p_l(\mathbf{x}^s)\Lambda(\mathbf{x}^s) \right\} \mathrm{d}x_1^s \tag{85}$$

$$\sigma_{ij}(\mathbf{x}) = \int_a^b \left\{ S_{lij}^*(\mathbf{x},\mathbf{x}^s)\, p_l(\mathbf{x}^s)\Lambda(\mathbf{x}^s) \right\} \mathrm{d}x_1^s \tag{86}$$

which can be evaluated by numerical integration techniques.

3. Hybrid finite element and special elements

If an arbitrary polygonal element e is taken into consideration, as shown in Figure 10, the hybrid variational functional Π_{me} at element level based on two-field approximations is given by

$$\Pi_{me} = \frac{1}{2}\int_{\Omega_e} \boldsymbol{\sigma}^{\mathrm{T}}\boldsymbol{\varepsilon}\mathrm{d}\Omega - \int_{\Omega_e} \mathbf{b}^{\mathrm{T}}\mathbf{u}\mathrm{d}\Omega - \int_{\Gamma_e^s} \bar{\mathbf{s}}^{\mathrm{T}} \tilde{\ } \cdots \int_{\Gamma_e} \cdots$$

(87)

where Ω_e is the element domain under consideration and Γ_e is its boundary, and

$$\mathbf{u} = \{u_1 \quad u_2\}^{\mathrm{T}}, \quad \cdots = \{b_1 \quad b_2\}^{\mathrm{T}}$$
$$\boldsymbol{\sigma} = \{\sigma_{11} \quad \sigma_{22} \quad \sigma_{12}\}^{\mathrm{T}}, \quad \boldsymbol{\varepsilon} = \{\varepsilon_{11} \quad \varepsilon_{22} \quad \gamma_{12}\}^{\mathrm{T}}, \quad \mathbf{s} = \{s_1 \quad s_2\}^{\mathrm{T}} \tag{88}$$

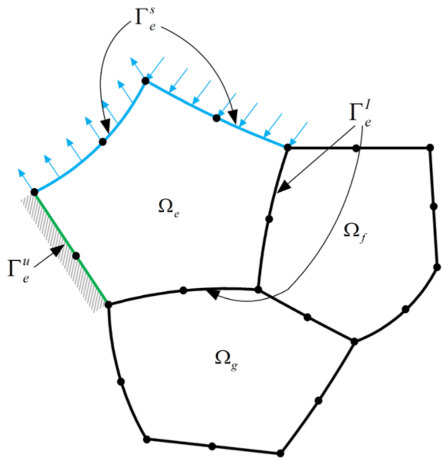

Figure 10. Schematic of arbitrary polygonal element

In Eq. (88), **u**, **σ** and **ε** are respectively displacement, stress, and strain column vectors defined within the element domain Ω_e, while $\tilde{\ }$ is an independent displacement vector defined along the element boundary Γ_e. **s** denotes the element traction vector, and $\bar{\mathbf{s}}$ is the specified value of it applied on the portion Γ_e^s of the element boundary. Besides, in Figure 10, Γ_e^I and Γ_e^u are common boundaries of adjacent elements, for instance, elements e and f or g, and the boundary with specified displacement constraint. For a well-posed element, we have

$$\Gamma_e = \Gamma_e^u + \Gamma_e^s + \Gamma_e^I \tag{89}$$

If the interior element approximation is required to satisfy exactly the governing Eq. (71), then applying the Gaussian theorem to the functional above we have the following simplified expression of the functional

$$\Pi_{me} = -\frac{1}{2}\int_{\Gamma_e} \mathbf{u}^{\mathrm{T}}\mathbf{s}\mathrm{d}\Gamma - \frac{1}{2}\int_{\Omega_e} \mathbf{b}^{\mathrm{T}}\mathbf{u}\mathrm{d}\Omega - \int_{\Gamma_e^s} \bar{\mathbf{s}}^{\mathrm{T}} \cdots \int_{\Gamma_e} \cdots \tag{90}$$

Here, two types of elements are discussed. One is the general hybrid element established with fundamental solution approximation in the absence of body forces, and the other is the special hybrid element in which the fundamental solution approximations used in general elements are augmented with the suitable local solutions to accurately capture the local effects due to the discontinuous loads and then to avoid the troublesome of mesh refinement near the region over which the discontinuous loads are applied. In what follows, detailed derivation of the special element is presented.

The generalized body forces corresponding to point and line loads are rewritten in a unified form as

$$\mathbf{b}(\mathbf{x}) = \begin{cases} \{P_1 \quad P_2\}^{\mathrm{T}} \delta(\mathbf{x}, \mathbf{x}_0^s) & \text{for point-load} \\ \int_{L_{AB}} \{p_1(\mathbf{x}^s) \quad p_2(\mathbf{x}^s)\}^{\mathrm{T}} \delta(\mathbf{x}, \mathbf{x}^s)\mathrm{d}L & \text{for line-load} \end{cases} \tag{91}$$

Subsequently, the second integral in the variational functional (90) can be written

$$\int_{\Omega_e} \mathbf{b}^{\mathrm{T}}\mathbf{u}\mathrm{d}\Omega = \begin{cases} \{P_1 \quad P_2\}\mathbf{u}(\mathbf{x}_0^s) & \text{for point-load} \\ \int_{L_{AB}} \{p_1(\mathbf{x}^s) \quad p_2(\mathbf{x}^s)\}\mathbf{u}(\mathbf{x}^s)\mathrm{d}L & \text{for line-load} \end{cases}$$

(92)

where the properties of the delta function have been employed.

If the load intensity of a line load is assumed to be constant, that is, p_i are constant, then Eq. (92) can be reduced to

$$\int_{\Omega_e} \mathbf{b}^{\mathrm{T}}\mathbf{u}\mathrm{d}\Omega = \begin{cases} \mathbf{P}_0^{\mathrm{T}}\mathbf{u}(\mathbf{x}_0^s) & \text{for point-load case} \\ \mathbf{P}_0^{\mathrm{T}}\int_{L_{AB}} \mathbf{u}(\mathbf{x}^s)\mathrm{d}L & \text{for line-load case} \end{cases} \tag{93}$$

where

$$\mathbf{P}_0 = \{P_1 \quad P_2\}^{\mathrm{T}} \tag{94}$$

for the case of concentrated forces, and

$$\mathbf{P}_0 = \{p_1 \quad p_2\}^{\mathrm{T}} \tag{95}$$

For the case of line loads

III. CONCLUSION

Based on the preceding discussion, the following conclusions can be drawn. This review reports recent developments on special hybrid H-Trefftz and F-Trefftz FEM. It proved to be a powerful computational tool in modeling materials and structures with various mechanical properties. However, there are still many possible extensions and areas in need of further development in the future. Among those developments one could list the following:

1. Development of efficient F-Trefftz FE-BEM schemes for complex engineering structures containing heterogeneous materials and the related general purpose computer codes with preprocessing and postprocessing capabilities.
2. Generation of various special-purpose elements to effectively handle singularities attributable to local geometrical or load effects (holes, cracks, inclusions, interface, corner and load singularities). The special-purpose functions warrant that excellent results are obtained at minimal computational cost and without local mesh refinement.
3. Development of F-Trefftz FE in conjunction with a topology optimization scheme to contribute to microstructure design.
4. Extension of the F-Trefftz FEM to elastodynamics and fracture mechanics of FGMs.

IV. REFERENCES

[1]. L. Yin, S. Venkatesan, D. Webb, S. Kalyanasundaram, Q.H. Qin, M.R. Forwood, Mechanical responses of hydrated and dehydrated cortical bones to microindentation, in: Proceedings of the 6th Australasian Congress on Applied Mechanics, Engineers Australia, 2010, pp. 1033.

[2]. S. Venkatesan, L. Yin, S. Kalyanasundaram, Q.H. Qin, A study on the real time strain measurement system for analysis of strain evolution and failure behavior of cortical bone materials, in: Proceedings of 2nd Asia Pacific Workshop on Structural Health Monitoring, September 1st, 2008., Materials Forum, vol. 33, 2009, pp. 46-52.

[3]. C.-Y. Qu, Q.H. Qin, Y.L. Kang, Theoretical prediction of surface bone remodeling under axial and transverse loads, in: Proc. of 9th International Conference on Inspection, Appraisal, Repairs & Maintenance of Structures, Fuzhou, China, 20-21 October, CI-Premier PTY LTD, ISBN: 981-05-3548-1, 2005, pp. 373-380.

[4]. N. Nasiri, T.D. Elmøe, Q.H. Qin, A. Tricoli, Aerosol self-assembly of nanoparticle films: growth dynamics and resulting 3D structure, in: Fourth International Conference on Smart Materials and Nanotechnology in Engineering,

International Society for Optics and Photonics, 2013, pp. 879320-879320-879326.
[5]. D. Li, Q.H. Qin, Y. Xiao, D. Zuo, W. Lu, Crack and defect formation in diamond films, in: 13th International Conference of fracture, June 16–21, 2013, Beijing, China, 2013.
[6]. Q.H. Qin, Mechanics of Cellular Bone Remodeling: Coupled Thermal, Electrical, and Mechanical Field Effects, in, CRC Press, Taylor & Francis, Boca Raton, 2013.
[7]. Q.H. Qin, Y.W. Mai, A closed crack tip model for interface cracks in thermopiezoelectric materials, International Journal of Solids and Structures, 36(16) (1999) 2463-2479.
[8]. S.W. Yu, Q.H. Qin, Damage analysis of thermopiezoelectric properties: Part II. Effective crack model, Theoretical and Applied Fracture Mechanics, 25(3) (1996) 279-288.
[9]. Q.H. Qin, 2D Green's functions of defective magnetoelectroelastic solids under thermal loading, Engineering Analysis with Boundary Elements, 29(6) (2005) 577-585.
[10]. Q.H. Qin, General solutions for thermopiezoelectrics with various holes under thermal loading, International Journal of Solids and Structures, 37(39) (2000) 5561-5578.
[11]. Q.H. Qin, Green's function and boundary elements of multifield materials, Elsevier, Oxford, 2007.
[12]. Q.H. Qin, Y.W. Mai, S.W. Yu, Some problems in plane thermopiezoelectric materials with holes, International Journal of Solids and Structures, 36(3) (1999) 427-439.
[13]. Q.H. Qin, Y.W. Mai, Crack growth prediction of an inclined crack in a half-plane thermopiezoelectric solid, Theoretical and Applied Fracture Mechanics, 26(3) (1997) 185-191.
[14]. Q.H. Qin, Fracture mechanics of piezoelectric materials, WIT Press, Southampton, 2001.
[15]. Q.H. Qin, S.W. Yu, An arbitrarily-oriented plane crack terminating at the interface between dissimilar piezoelectric materials, International Journal of Solids and Structures, 34(5) (1997) 581-590.
[16]. S.W. Yu, Q.H. Qin, Damage analysis of thermopiezoelectric properties: Part I—crack tip singularities, Theoretical and Applied Fracture Mechanics, 25(3) (1996) 263-277.
[17]. J.S. Wang, G.F. Wang, X.Q. Feng, Q.H. Qin, Surface effects on the superelasticity of nanohelices, Journal of Physics: Condensed Matter, 24(26) (2012) 265303.
[18]. J.S. Wang, X.Q. Feng, J. Xu, Q.H. Qin, S.W. Yu, Chirality transfer from molecular to morphological scales in quasi-one-dimensional nanomaterials: a continuum model, Journal of Computational and Theoretical Nanoscience, 8(7) (2011) 1278-1287.
[19]. J.-S. Wang, G.-F. Wang, X.-Q. Feng, Q.H. Qin, Surface effects on the superelasticity of nanohelices, Journal of Physics: Condensed Matter, 24(26) (2012) 265303.
[20]. Y. Wang, Q.H. Qin, S. Kalyanasundaram, A theoretical model for simulating effect of parathyroid hormone on bone metabolism at cellular level, Molecular & Cellular Biomechanics, 6 (2009) 101-112.
[21]. Q.H. Qin, Y.-W. Mai, Crack path selection in piezoelectric bimaterials, Composite structures, 47(1) (1999) 519-524.
[22]. H. Wang, Q.H. Qin, Y. Xiao, Special n-sided Voronoi fiber/matrix elements for clustering thermal effect in natural-hemp-fiber-filled cement composites, International Journal of Heat and Mass Transfer, 92 (2016) 228-235.
[23]. Q.H. Qin, The Trefftz finite and boundary element method, WIT Press, Southampton, 2000.
[24]. Q.H. Qin, Trefftz finite element method and its applications, Applied Mechanics Reviews, 58(5) (2005) 316-337.
[25]. H. Wang, Q.H. Qin, Y. Kang, A meshless model for transient heat conduction in functionally graded materials, Computational Mechanics, 38(1) (2006) 51-60.
[26]. N. Bavi, Q.H. Qin, B. Martinac, Finite element simulation of the gating mechanism of mechanosensitive ion channels, in: Fourth International Conference on Smart Materials and Nanotechnology in Engineering, International Society for Optics and Photonics, 2013, pp. 87931S-87931S-87937.
[27]. C. Liu, Y. Zhang, Q.H. Qin, R.B. Heslehurst, Numerical Modelling of Glass Fibre Metal Laminates Subjected to High Velocity Impact, in: Proceedings of the Composites Australia and CRC-ACS, 2013 Composites Conference (Edited by Rikard Heslehurst), Melbourne, 4-5 March 2013, 2013.

[28]. C.J. Liu, Y. Zhang, Q.H. Qin, R. Heslehurst, High velocity impact modelling of sandwich panels with aluminium foam core and aluminium sheet skins, in: Applied Mechanics and Materials, 2014, pp. 745-750.
[29]. Z.J. Fu, Q.H. Qin, W. Chen, Hybrid-Trefftz finite element method for heat conduction in nonlinear functionally graded materials, Engineering Computations, 28(5) (2011) 578-599.
[30]. Q.H. Qin, H. Wang, Matlab and C programming for Trefftz finite element methods, New York: CRC Press, 2008.
[31]. Q.H. Qin, C.X. Mao, Coupled torsional-flexural vibration of shaft systems in mechanical engineering—I. Finite element model, Computers & Structures, 58(4) (1996) 835-843.
[32]. H.C. Martin, G.F. Carey, Introduction to finite element analysis: Theory and application, McGraw-Hill New York, 1973.
[33]. H. Wang, Y. Xiao, Q.H. Qin, 2D hierarchical heat transfer computational model of natural ber bundle reinforced composite, Scientia Iranica, Transactions B: Mechanical Engineering, 23(1) (2016) 268-276.
[34]. K.Z. Ding, Q.H. Qin, M. Cardew-Hall, A New Integration Algorithm for the Finite Element Analysis of Elastic-Plastic Problems, in: Proc. of 9th International Conference on Inspection, Appraisal, Repairs & Maintenance of Structures, Fuzhou, China, 20-21 October, CI-Premier PTY LTD, ISBN: 981-05-3548-1, 2005, pp. 209-216.
[35]. Q.H. Qin, Y.W. Mai, BEM for crack-hole problems in thermopiezoelectric materials, Engineering Fracture Mechanics, 69(5) (2002) 577-588.
[36]. Q.H. Qin, Y. Huang, BEM of postbuckling analysis of thin plates, Applied Mathematical Modelling, 14(10) (1990) 544-548.
[37]. Q.H. Qin, Nonlinear analysis of Reissner plates on an elastic foundation by the BEM, International journal of solids and structures, 30(22) (1993) 3101-3111.
[38]. W. Chen, Z.-J. Fu, Q.-H. Qin, Boundary particle method with high-order Trefftz functions, Computers, Materials & Continua (CMC), 13(3) (2010) 201-217.
[39]. H. Wang, Q.H. Qin, D. Arounsavat, Application of hybrid Trefftz finite element method to non-linear problems of minimal surface, International Journal for Numerical Methods in Engineering, 69(6) (2007) 1262-1277.
[40]. H. Wang, Q.H. Qin, X.-P. Liang, Solving the nonlinear Poisson-type problems with F-Trefftz hybrid finite element model, Engineering Analysis with Boundary Elements, 36(1) (2012) 39-46.
[41]. L.L. Cao, Q.H. Qin, N. Zhao, A new RBF-Trefftz meshless method for partial differential equations, IOP Conference Series: Materials Science and Engineering, 10 (2010) 012217.
[42]. Q.H. Qin, Dual variational formulation for Trefftz finite element method of elastic materials, Mechanics Research Communications, 31(3) (2004) 321-330.
[43]. H. Wang, Q.H. Qin, Numerical implementation of local effects due to two-dimensional discontinuous loads using special elements based on boundary integrals, Engineering Analysis with Boundary Elements, 36(12) (2012) 1733-1745.
[44]. Q.H. Qin, Formulation of hybrid Trefftz finite element method for elastoplasticity, Applied Mathematical Modelling, 29(3) (2005) 235-252.
[45]. Q.H. Qin, Trefftz plane elements of elastoplasticity with p-extension capabilities, Journal of Mechanical Engineering, 56(1) (2005) 40-59.
[46]. Y. Cui, Q.H. Qin, Fracture analysis of mode III problems by Trefftz finite element approach, in: WCCM VI in conjunction with APCOM, 2004, pp. v1-p380.
[47]. Y.-h. Cui, Q.H. Qin, J.-S. Wang, Application of HT finite element method to multiple crack problems of Mode I, II and III, Chinese Journal of Engineering Mechanics, 23(3) (2006) 104-110.
[48]. Y. Cui, J. Wang, M. Dhanasek, Q.H. Qin, Mode III fracture analysis by Trefftz boundary element method, Acta Mechanica Sinica, 23(2) (2007) 173-181.
[49]. C. Cao, Q.H. Qin, A. Yu, Micromechanical Analysis of Heterogeneous Composites using Hybrid Trefftz FEM and Hybrid Fundamental Solution Based FEM, Journal of Mechanics, 29(4) (2013) 661-674.
[50]. C. Cao, A. Yu, Q.H. Qin, Evaluation of effective thermal conductivity of fiber-reinforced composites by boundary integral based finite element method, International Journal of Architecture, Engineering and Construction, 1(1) (2012) 14-29.

[51]. M. Dhanasekar, J. Han, Q.H. Qin, A hybrid-Trefftz element containing an elliptic hole, Finite Elements in Analysis and Design, 42(14) (2006) 1314-1323.
[52]. Q.H. Qin, X.Q. He, Special elliptic hole elements of Trefftz FEM in stress concentration analysis, Journal of Mechanics and MEMS, 1(2) (2009) 335-348.
[53]. J. Jirousek, Q.H. Qin, Application of hybrid-Trefftz element approach to transient heat conduction analysis, Computers & Structures, 58(1) (1996) 195-201.
[54]. L. Cao, Q.H. Qin, N. Zhao, Application of DRM-Trefftz and DRM-MFS to Transient Heat Conduction Analysis, Recent Patents on Space Technology (Open access), 2 (2010) 41-50.
[55]. N. Zhao, L.L. Cao, Q.H. Qin, Application of Trefftz Method to Heat Conduction Problem in Functionally Graded Materials, Recent Patents on Space Technology, 1(2) (2011) 158-166.
[56]. Q.H. Qin, Hybrid Trefftz finite-element approach for plate bending on an elastic foundation, Applied Mathematical Modelling, 18(6) (1994) 334-339.
[57]. Q.H. Qin, Postbuckling analysis of thin plates by a hybrid Trefftz finite element method, Computer Methods in Applied Mechanics and Engineering, 128(1) (1995) 123-136.
[58]. Q.H. Qin, Transient plate bending analysis by hybrid Trefftz element approach, Communications in Numerical Methods in Engineering, 12(10) (1996) 609-616.
[59]. Q.H. Qin, Postbuckling analysis of thin plates on an elastic foundation by HT FE approach, Applied Mathematical Modelling, 21(9) (1997) 547-556.
[60]. F. Jin, Q.H. Qin, A variational principle and hybrid Trefftz finite element for the analysis of Reissner plates, Computers & Structures, 56(4) (1995) 697-701.
[61]. J. Jirousek, A. Wroblewski, Q.H. Qin, X. He, A family of quadrilateral hybrid-Trefftz p-elements for thick plate analysis, Computer Methods in Applied Mechanics and Engineering, 127(1) (1995) 315-344.
[62]. Q.H. Qin, Hybrid-Trefftz Finite-Element Method for Reissner Plates on an Elastic-Foundation, Computer Methods in Applied Mechanics and Engineering, 122(3-4) (1995) 379-392.
[63]. Q.H. Qin, S. Diao, Nonlinear analysis of thick plates on an elastic foundation by HT FE with p-extension capabilities, International Journal of Solids and Structures, 33(30) (1996) 4583-4604.
[64]. Q.H. Qin, Nonlinear analysis of thick plates by HT FE approach, Computers & Structures, 61(2) (1996) 271-281.
[65]. C.-Y. Lee, Q.H. Qin, H. Wang, Trefftz functions and application to 3D elasticity, Computer Assisted Mechanics and Engineering Sciences, 15 (2008) 251-263.
[66]. Q.H. Qin, Variational formulations for TFEM of piezoelectricity, International Journal of Solids and Structures, 40(23) (2003) 6335-6346.
[67]. Q.H. Qin, Solving anti-plane problems of piezoelectric materials by the Trefftz finite element approach, Computational Mechanics, 31(6) (2003) 461-468.
[68]. Q.H. Qin, Mode III fracture analysis of piezoelectric materials by Trefftz BEM, Structural Engineering and Mechanics, 20(2) (2005) 225-240.
[69]. Q.H. Qin, Fracture Analysis of Piezoelectric Materials by Boundary and Trefftz Finite Element Methods, WCCM VI in conjunction with APCOM'04, Sept. 5-10, 2004, Beijing, China, (2004).
[70]. Q.H. Qin, Trefftz Plane Element of Piezoelectric Plate with p-Extension Capabilities, IUTAM Symposium on Mechanics and Reliability of Actuating Materials, (2006) 144-153.
[71]. Q.H. Qin, K.-Y. Wang, Application of hybrid-Trefftz finite element method fractional contact problems, Computer Assisted Mechanics and Engineering Sciences, 15 (2008) 319-336.
[72]. K. Wang, Q.H. Qin, Y. Kang, J. Wang, C. Qu, A direct constraint-Trefftz FEM for analysing elastic contact problems, International Journal for Numerical Methods in Engineering, 63(12) (2005) 1694-1718.
[73]. M. Dhanasekar, K.Y. Wang, Q.H. Qin, Y.L. Kang, Contact analysis using Trefftz and interface finite elements, Computer Assisted Mechanics and Engineering Sciences, 13(3) (2006) 457-471.
[74]. H. Wang, Q.H. Qin, Hybrid FEM with fundamental solutions as trial functions for heat conduction simulation, Acta Mechanica Solida Sinica, 22(5) (2009) 487-498.
[75]. C. Cao, Q.H. Qin, Hybrid fundamental solution based finite element method: theory and applications, Advances in Mathematical Physics, 2015 (2015).

[76]. Q.H. Qin, Fundamental Solution Based Finite Element Method, J Appl Mech Eng, 2 (2013) e118.

[77]. Z.-J. Fu, W. Chen, Q.H. Qin, Hybrid Finite Element Method Based on Novel General Solutions for Helmholtz-Type Problems, Computers Materials and Continua, 21(3) (2011) 187.

[78]. Y.-T. Gao, H. Wang, Q.H. Qin, Orthotropic Seepage Analysis using Hybrid Finite Element Method, Journal of Advanced Mechanical Engineering, 2(1) (2015) 1-13.

[79]. H. Wang, Q.H. Qin, Fundamental solution-based hybrid finite element analysis for non-linear minimal surface problems, Recent Developments in Boundary Element Methods: A Volume to Honour Professor John T. Katsikadelis, 309 (2010).

[80]. H. Wang, Q.H. Qin, Fundamental-solution-based hybrid FEM for plane elasticity with special elements, Computational Mechanics, 48(5) (2011) 515-528.

[81]. H. Wang, Q.H. Qin, W. Yao, Improving accuracy of opening-mode stress intensity factor in two-dimensional media using fundamental solution based finite element model, Australian Journal of Mechanical Engineering, 10(1) (2012) 41-51.

[82]. Q.H. Qin, H. Wang, Special Elements for Composites Containing Hexagonal and Circular Fibers, International Journal of Computational Methods, 12(04) (2015) 1540012.

[83]. H. Wang, Q.H. Qin, Special fiber elements for thermal analysis of fiber-reinforced composites, Engineering Computations, 28(8) (2011) 1079-1097.

[84]. H. Wang, Q.H. Qin, A fundamental solution based FE model for thermal analysis of nanocomposites, in: Boundary elements and other mesh Reduction methods XXXIII', 33rd International Conference on Boundary Elements and other Mesh Reduction Methods, ed. CA Brebbia and V. Popov, WIT Press, UK, 2011, pp. 191-202.

[85]. H. Wang, Q.H. Qin, Implementation of fundamental-solution based hybrid finite element model for elastic circular inclusions, in: Proceedings of the Asia-Pacific Congress for Computational Mechanics, 11th-14th Dec, 2013.

[86]. C. Cao, Q.H. Qin, A. Yu, Modelling of Anisotropic Composites by Newly Developed HFS-FEM, in: Proceedings of the 23rd International Congress of Theoretical and Applied Mechanics, Yilong Bai , Jianxiang Wang , Daining Fang (eds), SM08-016, August 19 - 24 , 2012, Beijing, China, The International Union of Theoretical and Applied Mechanics (IUTAM), 2012.

[87]. H. Wang, Q.H. Qin, Advanced Fundamental-solution-based Computational Methods for Thermal Analysis of Heterogeneous Materials, in: Advanced Engineering Materials and Modelling, WILEY-Scrivener Publishing, 2016, pp. 331-368.

[88]. C. Cao, Q.H. Qin, A. Yu, Hybrid fundamental-solution-based FEM for piezoelectric materials, Computational Mechanics, 50(4) (2012) 397-412.

[89]. C. Cao, A. Yu, Q.-H. Qin, A new hybrid finite element approach for plane piezoelectricity with defects, Acta Mechanica, 224(1) (2013) 41-61.

[90]. H. Wang, Q.H. Qin, Fracture analysis in plane piezoelectric media using hybrid finite element model, in: International Conference of fracture, 2013.

[91]. C. Cao, Q.H. Qin, A. Yu, A new hybrid finite element approach for three-dimensional elastic problems, Archives of Mechanics, 64(3) (2012) 261-292.

[92]. L.-L. Cao, Q.H. Qin, N. Zhao, Hybrid graded element model for transient heat conduction in functionally graded materials, Acta Mechanica Sinica, 28(1) (2012) 128-139.

[93]. L. Cao, H. Wang, Q.H. Qin, Fundamental solution based graded element model for steady-state heat transfer in FGM, Acta Mechanica Solida Sinica, 25(4) (2012) 377-392.

[94]. H. Wang, Q.H. Qin, Boundary integral based graded element for elastic analysis of 2D functionally graded plates, European Journal of Mechanics-A/Solids, 33 (2012) 12-23.

[95]. H. Wang, Q.H. Qin, FE approach with Green's function as internal trial function for simulating bioheat transfer in the human eye, Archives of Mechanics, 62(6) (2010) 493-510.

[96]. H. Wang, Q.H. Qin, Computational bioheat modeling in human eye with local blood perfusion effect, Human Eye Imaging and Modeling, (2012).

[97]. H. Wang, Q.H. Qin, A fundamental solution-based finite element model for analyzing multi-layer skin burn injury, Journal of Mechanics in Medicine and Biology, 12(05) (2012) 1250027.

[98]. Z.-W. Zhang, H. Wang, Q.H. Qin, Transient bioheat simulation of the laser-tissue interaction in human skin using hybrid finite element formulation, Molecular & Cellular Biomechanics, 9(1) (2012) 31-53.
[99]. Z.W. Zhang, H. Wang, Q.H. Qin, Analysis of transient bioheat transfer in the human eye using hybrid finite element model, in: Applied Mechanics and Materials, Trans Tech Publ, 2014, pp. 356-361.
[100].J. Tao, Q.H. Qin, L. Cao, A Combination of Laplace Transform and Meshless Method for Analysing Thermal Behaviour of Skin Tissues, Universal Journal of Mechanical Engineering, 1(2) (2013) 32-42.
[101].Z.W. Zhang, H. Wang, Q.H. Qin, Method of fundamental solutions for nonlinear skin bioheat model, Journal of Mechanics in Medicine and Biology, 14(4) (2014) 1450060.
[102].C. Cao, Q.H. Qin, A. Yu, A novel boundary-integral based finite element method for 2D and 3D thermo-elasticity problems, Journal of Thermal Stresses, 35(10) (2012) 849-876.
[103].Q.H. Qin, H. Wang, Special circular hole elements for thermal analysis in cellular solids with multiple circular holes, International Journal of Computational Methods, 10(04) (2013) 1350008.
[104].H. Wang, Q.H. Qin, A new special element for stress concentration analysis of a plate with elliptical holes, Acta Mechanica, 223(6) (2012) 1323-1340.
[105].Q.H. Qin, H. Wang, Fundamental solution based FEM for nonlinear thermal radiation problem, in: 12th International Conference on Boundary Element and Meshless Techniques (BeTeq 2011), ed. EL Albuquerque, MH Aliabadi, EC Ltd, Eastleigh, UK, 2011, pp. 113-118.
[106].C. Cao, A. Yu, Q.H. Qin, A novel hybrid finite element model for modeling anisotropic composites, Finite Elements in Analysis and Design, 64 (2013) 36-47.
[107].C. Cao, A. Yu, Q.H. Qin, Mesh reduction strategy: Special element for modelling anisotropic materials with defects, Boundary Elements and Other Mesh Reduction Methods XXXVI, 56 (2013) 61.
[108].H. Wang, Q.H. Qin, Fundamental-solution-based finite element model for plane orthotropic elastic bodies, European Journal of Mechanics-A/Solids, 29(5) (2010) 801-809.
[109].H. Wang, Q.H. Qin, Y.P. Lei, Green's-function-based-finite element analysis of fully plane anisotropic elastic bodies, Journal of Mechanical Science and Technology, 31(3) (2017) 1305-1313.
[110].N.I. Muskhelishvili, Some basic problems of the mathematical theory of elasticity, Springer Science & Business Media, 2013.